PERGAMON

Deep-Sea Research I 48 (2001) 1423–1441

DEEP-SEA RESEARCH
PART I

www.elsevier.com/locate/dsr

Age tracers in an ocean GCM

S. Khatiwala*, M. Visbeck, P. Schlosser

Lamont–Doherty Earth Observatory and Department of Earth and Environmental Sciences, Columbia University, Palisades, NY 10964, USA

Received 31 March 2000; received in revised form 5 September 2000; accepted 2 October 2000

Abstract

Observations of transient tracers such as tritium and helium-3 (^{3}He) are frequently combined to construct "age-like" quantities generally interpreted to represent time elapsed since a fluid parcel was last at the surface. In a turbulent ("diffusive") environment such as the ocean, we must regard the fluid parcel as being composed of material fluid elements that have spent different lengths of time since their last contact with the surface. Hence, they are characterized by an age spectrum or distribution of transit times. In this study we explore the concepts of tracer-derived "ages" and the transit-time probability density function (PDF) with the aim of improving our understanding of their interpretation. Using an ocean general circulation model, we illustrate the effect of mixing on tracer-derived "ages" within the Atlantic Ocean. The mixing biases such ages towards younger values with respect to the ideal or mean age of a water parcel. In the North Atlantic, this bias is particularly pronounced in the thermocline because of large vertical gradients in tracer concentration, and in the deep ocean, where the penetration of recently ventilated water creates large gradients along the isopycnal surfaces. In contrast, the effect of mixing appears to be relatively small in the subtropical subduction region. Calculations of the transit-time PDF in the ocean model show, however, that the mean age can potentially be very large because of contributions from long transit-time pathways, in spite of the fact that such pathways make up a small fraction of the fluid parcel. These results illustrate the key idea that tracer-derived ages are weighted towards the leading part of the transit-time distribution, while the ideal age is more sensitive to its "tail". These tracers are thus sensitive to and help constrain different time scales. We also find that the ideal age converges much more rapidly to the mean age compared with the first moment of the age spectrum, an important consideration in numerical studies. © 2001 Elsevier Science Ltd. All rights reserved.

Keywords: Radioactive tracers; Dyes; Residence time; Water circulation; Transit time; Age spectrum

* Corresponding author. Present address: Department of Earth, Atmospheric and Planetary Sciences, Massachusetts Institute of Technology, Cambridge, MA 02139, USA. Fax: + 617-253-4464.

E-mail address: spk@ocean.mit.edu (S. Khatiwala).

0967-0637/01/$ - see front matter © 2001 Elsevier Science Ltd. All rights reserved.
PII: S0967-0637(00)00094-7

1. Introduction

Transient tracers such as tritium (^3H), ^3He and chlorofluorocarbons (CFC's) can potentially give us valuable information on the time scales on which the ocean is ventilated. These tracers are often used to compute an "age" which, ideally, represents the time elapsed since a water parcel was last at the surface. The interpretation of such tracer-derived "ages", however, is complicated by the fact that the ocean is a diffusive environment and tracer ages are not conservative with respect to mixing. On the other hand, the advantage of tracer-derived ages (such as the tritium–^3He age) is that they are independent of (poorly known) boundary conditions. Thus, their simplicity (requiring only a knowledge of in situ concentrations) has led to their widespread use in the oceanographic community.

One immediate conceptual problem that we face when constructing an "age" from observed tracer concentrations is that a water parcel in a diffusive geophysical flow is in fact characterized by an age spectrum (Kida, 1983; Hall and Plumb, 1994). For example, if we are interested in the "ventilation" of the ocean, then we must regard the parcel as being composed of material fluid elements that have spent different lengths of time since their last contact with the surface. The age spectrum or probability density function of transit times captures this information.

In this paper we present some results from the integration of an ocean general circulation model (OGCM) in which a number of age tracers were simulated. The goal of these numerical experiments is to gain insight into the interpretation of transient-tracer ages. In particular, we highlight the effect of mixing on various measures of "age". One frequently cited "problem" with tritium–^3He ages is that they are biased towards the age of the youngest "component". Note that the term "component", although widely used in the literature (and above to make a point), is ill-defined in the presence of mixing. Indeed, in this study we wish to move away from such usage and recognize the *continuous* nature of the age spectrum. The "problem" mentioned above is really in the choice of an appropriate time scale with which to compare transient-tracer ages (cf. Jenkins, 1998). Thus, comparing the tritium–^3He age with an ideal age tracer, we argue that the bias of tritium–helium ages towards younger values is in fact a useful property from an oceanographic point of view. We also present numerical calculations of the transit-time PDF in the OGCM. A comparison with conventional tracer-derived ages shows that the transit-time PDF is a potentially powerful tool to aid in the interpretation of tracer-derived ages.

2. Description of "age" tracers

2.1. Tritium and helium

Tritium was produced during atmospheric nuclear weapons tests, mainly in the early 1960s, and injected into the stratosphere. This tritium was oxidized to HTO and delivered to the ocean surface via vapor exchange, precipitation, and rivers. Thus, as a result of its time-dependent delivery to the surface waters, tritium can be used as a "dye" tracer to study the penetration and spreading of surface waters into the interior of the ocean. Tritium decays to ^3He with a half-life of 12.43 yr (Unterweger et al., 1980). At the surface, ^3He produced by ^3H decay is lost to the atmosphere by gas exchange. Thus tritium and ^3He may be combined to form a radioactive "clock" which is reset at

the surface (e.g. Jenkins and Clarke, 1976). The ^{3}H–^{3}He age can be interpreted as the time elapsed since the water parcel was isolated from the surface (say, by convection). ^{3}H–^{3}He ages give us a first-order estimate of renewal rates and residence times. The ^{3}H–^{3}He age (τ_{th}) in years is given by

$$\tau_{th} = \lambda^{-1} \ln(1 + [^3\mathrm{He}]/[^3\mathrm{H}]), \tag{1}$$

where λ is the decay constant for ^{3}H. Because the ^{3}H–^{3}He age is a non-linear function of ^{3}H and ^{3}He concentrations, the ^{3}H–^{3}He ages are not conservative with respect to mixing and are typically biased towards younger values. For example, a mixture of "recently" ventilated water and "old" tracer-*free* water will have a ^{3}H–^{3}He age equal to that of the younger fraction.

This behavior of ages based on tracer ratios raises the following questions:

- Is the age "bias" significant?
- If so, how large is it, and where in the ocean is it important?
- What do we compare tracer-derived ages to?

2.2. Ideal age tracer

The ideal or mean age is a frequently utilized "benchmark" for ventilation time against which tracer-derived ages are compared (e.g., Thiele and Sarmiento, 1990; England, 1995). The governing equation for ideal age (τ_{id}) is

$$\frac{D\tau_{id}}{Dt} = \kappa_h \nabla_h^2 \tau_{id} + \kappa_v \frac{\partial^2 \tau_{id}}{\partial z^2} + 1, \tag{2}$$

where the operator D/Dt is defined by

$$\frac{D}{Dt} = \frac{\partial}{\partial t} + \mathbf{V} \cdot \nabla. \tag{3}$$

κ_h and κ_v are the (constant) horizontal and vertical diffusivities, ∇_h^2 is the horizontal Laplacian operator, and $\mathbf{V}$ is the velocity field. Eq. (2) may be understood as follows: in the absence of diffusion the ideal age of a marked fluid particle ("Lagrangian age") increases by "1" per unit time. τ_{id} is conserved during mixing.

2.3. Effect of mixing on tracer ages

A simple interpretation of the ideal age tracer as a Lagrangian age is no longer valid in the presence of diffusion. But as discussed later, the ideal age can still be interpreted as the mean transit time. We illustrate the effect of mixing by a simple example. Consider a 1 : 1 mixture of 2 water parcels, A and B. Assume further that these parcels have only undergone advection from their formation site (an admittedly unrealistic scenario), so their τ_{th} and τ_{id} are identical. The calculated tracer and age values for their mixture are shown in Table 1. These results illustrate the fact that τ_{th} is generally biased towards younger values. τ_{id}, on the other hand, is "conserved" during mixing in the sense that it is the mean of individual ages. To be more precise, τ_{th} reflects the leading part of the transit-time PDF, while τ_{id} is more sensitive to the "tail" of the PDF, i.e. these tracers are

Table 1
A simple example to show the effect of mixing on age tracers

Tracer	Parcel A	Parcel B	Mixture
$[^3He]$	0.1	5	2.55
$[^3H]$	5	0.1	2.55
τ_{th}	0.36	70.5	12.4 yr
τ_{id}	0.36	70.5	35.4 yr

sensitive to and help constrain different time scales. To understand the effect of mixing on the ^3H–^3He age consider the advection–diffusion equation for τ_{th} (Jenkins, 1987):

$$\frac{D\tau_{th}}{Dt} = \kappa_h \nabla_h^2 \tau_{th} + \kappa_v \frac{\partial^2 \tau_{th}}{\partial z^2} + 1 + \kappa_h \mathbf{\nabla}_h \ln([^3H]\zeta) \cdot \mathbf{\nabla}_h \tau_{th} + \kappa_v \frac{\partial \ln([^3H]\zeta)}{\partial z} \frac{\partial \tau_{th}}{\partial z}, \tag{4}$$

where $\zeta = [^3H] + [^3He]$. In comparison with the equation for τ_{id} (Eq. (2)), that for τ_{th} (Eq. (4)) has two additional terms due to mixing and the non-linearity of the age equation (Eq. (1)). These terms are typically negative in the ocean. In numerical studies (where the ideal age can be simulated) the difference between ideal age and ^3H–^3He age can become large (in upwelling regions, for example), making it difficult to compare them. We note in passing that the non-linear nature of the above equation is a result of our combining two tracers in a non-linear manner (for example, by forming a ratio).

3. The age spectrum

While tracer-derived "ages" have proven useful in studying ocean ventilation, a more complete characterization of a water parcel is given by the age spectrum or transit-time PDF (we use these terms interchangeably). Consider a fluid parcel in the ocean (Fig. 1). The irreducible fluid elements constituting the parcel were transported to that location from a specified region (the surface, say) by the turbulent flow via a multiplicity of pathways, each associated with a (not necessarily unique) transit time. The age spectrum or transit-time PDF describes the probability that a fluid element has been in the flow for a certain amount of time since last having been in contact with the surface. It should be mentioned that the concepts of age and transit-time distributions are not new, but appear to have been reinvented a number of times in different fields. In the early literature (e.g., Bolin and Rodhe, 1973; Nir and Lewis, 1975; IAEA, 1986), they appear as applications of systems theory to the flow of tracers in natural reservoirs, and in particular groundwater. The focus of these earlier studies was on zero-dimensional systems (well-mixed boxes or "lumped elements" in the terminology of systems theory) although one-dimensional advective–dispersive systems were also discussed. More recently, the idea of an age spectrum has been employed in the context of the distribution of chemical tracers in the stratosphere (Kida, 1983; Hall and Plumb, 1994), while Beining and Roether (1996) have applied it to the evolution of CFC concentrations in the ocean.

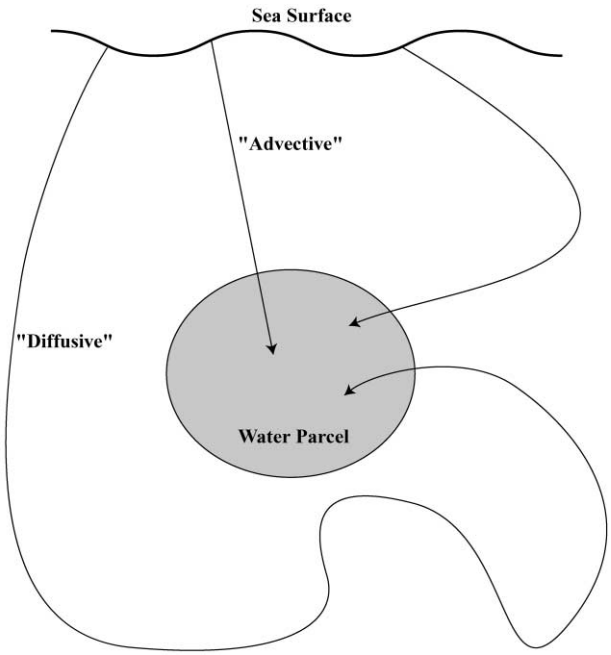

Fig. 1. Schematic illustrating the "advective" and "diffusive" pathways by which fluid elements constituting a water parcel are transported in the ocean.

The motivation for this study comes, in part, from the work of Holzer and Hall (2000), who have generalized and extended the theory in important ways by using the mathematical machinery of the Green's functions. We begin by briefly reviewing the basic ideas.

3.1. Solution of the advection–diffusion equation

The distribution $C(\mathbf{x}, t)$ of a passive tracer in the presence of a source, $Q(\mathbf{x}, t)$, can be modeled by

$$\frac{\partial C}{\partial t} + \mathscr{L}(C) = Q(\mathbf{x}, t), \tag{5}$$

where $\mathscr{L}$ is a (linear) transport operator, and $C(\mathbf{x}, t)$ is subject to prescribed initial conditions in the domain $\mathscr{D}$ and boundary conditions (BC's) on $\partial\mathscr{D}$. The transport operator that we consider is the advection–diffusion operator defined as

$$\mathscr{L} = \mathbf{V}(\mathbf{x}, t)\cdot\nabla - \nabla\cdot\kappa(\mathbf{x}, t)\nabla \tag{6}$$

Tracer is advected by the large-scale flow-field, $\mathbf{V}$, and "diffused" by the action of small-scale processes. In the context of ocean circulation models, the latter parameterizes unresolved processes.

Because of the linearity of $\mathscr{L}$, the solution to Eq. (5) can be expressed using standard techniques (e.g., Morse and Feshbach, 1953) as follows:

$$\begin{aligned} C(\mathbf{x},t) = & \int_0^t \mathrm{d}t' \iiint_{\mathscr{D}} \mathrm{d}^3x' G(\mathbf{x},t;\mathbf{x}',t') Q(\mathbf{x}',t') \\ & + \iiint_{\mathscr{D}} \mathrm{d}^3x' C(\mathbf{x}',0) G(\mathbf{x},t;\mathbf{x}',0) \\ & + \int_0^t \mathrm{d}t' \iint_{\partial\mathscr{D}} \mathrm{d}^2x' \{\kappa(\mathbf{x}',t')[G(\mathbf{x},t;\mathbf{x}',t')\nabla C(\mathbf{x}',t') \\ & - C(\mathbf{x}',t')\nabla G(\mathbf{x},t;\mathbf{x}',t')] - C(\mathbf{x}',t')G(\mathbf{x},t;\mathbf{x}',t')\mathbf{V}(\mathbf{x}',t')\} \cdot \hat{\mathbf{n}}, \end{aligned} \tag{7}$$

where $G(\mathbf{x},t;\mathbf{x}_\mathrm{o},t_\mathrm{o})$ is the Green's function satisfying

$$\left(\frac{\partial}{\partial t} + \mathscr{L}\right) G(\mathbf{x},t;\mathbf{x}_\mathrm{o},t_\mathrm{o}) = \delta(\mathbf{x}-\mathbf{x}_\mathrm{o})\delta(t-t_\mathrm{o}) \tag{8}$$

and δ is the multidimensional Dirac delta function. In deriving Eq. (7) we have imposed the conditions of causality and reciprocity on the Green's function. $G(\mathbf{x},t;\mathbf{x}_\mathrm{o},t_\mathrm{o})$ takes tracer injected at $(\mathbf{x}_\mathrm{o},t_\mathrm{o})$ to $(\mathbf{x},t)$ under the flow described by $\mathscr{L}$. Eq. (7) is the solution of the advection–diffusion equation with source term Q, initial condition $C(\mathbf{x},0)$ and boundary condition $C(\mathbf{x}_\mathrm{b},t)$ where $\mathbf{x}_\mathrm{b}$ is on $\partial\mathscr{D}$. Note how the Green's (or "influence") function propagates these inhomogeneous terms.

3.2. Boundary propagator

Eq. (7) expresses the solution in terms of the Green's function which is a solution to the transport equation for an impulse *source*. In certain circumstances, however, it is more useful to construct a solution using a function that satisfies impulse boundary conditions. In particular, Holzer and Hall (2001) define a *boundary propagator*, $G'(\mathbf{x},t;\mathbf{x}_\mathrm{o},t')$, which satisfies

$$\left(\frac{\partial}{\partial t} + \mathscr{L}\right) G'(\mathbf{x},t;\mathbf{x}_\mathrm{o},t')] = 0 \tag{9}$$

subject to the BC

$$G'(\mathbf{x}_\mathrm{b},t;\mathbf{x}_\mathrm{o},t') = \delta(\mathbf{x}_\mathrm{b}-\mathbf{x}_\mathrm{o})\delta(t-t'), \tag{10}$$

where $\mathbf{x}_\mathrm{b}$ and $\mathbf{x}_\mathrm{o}$ are points on $\partial\mathscr{D}$. The solution to Eq. (5) with $Q=0$ for a general BC, $C(\mathbf{x}_\mathrm{o},t)$, is then given by

$$C(\mathbf{x},t) = \int \mathrm{d}t' \iint_{\partial\mathscr{D}} \mathrm{d}^2x_\mathrm{o} G'(\mathbf{x},t;\mathbf{x}_\mathrm{o},t') C(\mathbf{x}_\mathrm{o},t'). \tag{11}$$

A causality condition holds for the boundary propagator such that $G'(\mathbf{x},t;\mathbf{x}_\mathrm{o},t')=0$ for $t<t'$. Holzer and Hall (2000) note that if $C(\mathbf{x}_\mathrm{o},t) = \Theta(t-t_\mathrm{o})$, where $\Theta(t)$ is the Heaviside step function, then the long-time ($t_\mathrm{o} \to -\infty$) solution to Eq. (11) is simply $C(\mathbf{x},t)=1$, i.e.,

$$\int_{-\infty}^t \mathrm{d}t' \iint_{\partial\mathscr{D}} \mathrm{d}^2x_\mathrm{o} G'(\mathbf{x},t;\mathbf{x}_\mathrm{o},t') = 1. \tag{12}$$

Based on the normalization, Eq. (12), the surface integral

$$\mathscr{G}'(\mathbf{x}, t; \partial\mathscr{D}, t') = \iint_{\partial\mathscr{D}} \mathrm{d}^2 x_\mathrm{o} G'(\mathbf{x}, t; \mathbf{x}_\mathrm{o}, t') \tag{13}$$

is interpreted as an "age spectrum", that is, a PDF of $\partial\mathscr{D}$-to-$\mathbf{x}$ transit times. Thus $\mathrm{d}\xi\mathscr{G}'(\mathbf{x}, t; \partial\mathscr{D}, t')$ is the probability that a fluid element at $(\mathbf{x}, t)$ had last contact with $\partial\mathscr{D}$ at a time between $\xi \equiv t - t'$ and $\xi + \mathrm{d}\xi$ ago. To make this clearer and establish the connection with Hall and Plumb (1994), consider the case of a stationary transport operator. Then the Green's function and boundary propagator can only depend on time through $\xi \equiv t - t'$. Furthermore, if the tracer boundary condition is independent of position, $C(\mathbf{x}_\mathrm{o}, t') = C_\mathrm{o}(t)$, then Eq. (11) can be rewritten as

$$C(\mathbf{x}, t) = \int_0^t \mathrm{d}\xi \mathscr{G}'(\mathbf{x}, \xi; \partial\mathscr{D}) C_\mathrm{o}(t - \xi). \tag{14}$$

This convolution integral has a straightforward interpretation. At time t the volume fraction of a fluid parcel at $\mathbf{x}$ which left the boundary at times between ξ and $\xi + \mathrm{d}\xi$ before t, and thus had a tracer concentration $C_\mathrm{o}(t - \xi)$, is simply $\mathrm{d}\xi\mathscr{G}'(\mathbf{x}, \xi; \partial\mathscr{D})$.

4. One-dimensional (1-d) simulations

Before going on to present results from the OGCM, we illustrate the concepts discussed so far in a simpler setting, that of the 1-d advection–diffusion equation for a passive tracer τ in a semi-infinite domain ($x > 0$), with constant velocity v, diffusivity κ, and source S. Nondimensionalizing via $x \to Lx$ and $t \to (L/v)t$, and defining a Peclet number $\mathrm{Pe} \equiv vL/\kappa$, where L is a typical length scale, the advection–diffusion equation becomes

$$\frac{\partial\tau}{\partial t} + \frac{\partial\tau}{\partial x} = \frac{1}{\mathrm{Pe}}\frac{\partial^2\tau}{\partial x^2} + S_\mathrm{o}, \tag{15}$$

where $S_\mathrm{o} = L/v$ when $\tau \equiv \tau_\mathrm{id}$, $S_\mathrm{o} = -\lambda\tau L/v$ when $\tau \equiv \theta([^3\mathrm{H}])$, and $S_\mathrm{o} = 0$ when $\tau \equiv \zeta([^3\mathrm{H}] + [^3\mathrm{He}])$. The boundary conditions at $x = 0$ are $\tau_\mathrm{id}(0, t) = 0$, $\theta(0, t) = 1$, and $\zeta(0, t) = 1$. Eq. (15) was solved numerically with the above source functions and boundary conditions using an implicit Cranck–Nicolson scheme. The boundary propagator, $G'(x, t)$, which in this case is also the transit-time PDF $\mathscr{G}'(x, t)$, also satisfies Eq. (15) with $S_\mathrm{o} = 0$, BC $G'(0, t) = \delta(t)$, and initial condition $G'(x,0) = 0$. We note that in the atmospheric context, Hall and Plumb (1994) derive the boundary propagator for the 1-d diffusion equation in a fluid with density decreasing exponentially with height. Invoking the Laplace transform (Abramowitz and Stegun, 1965), the boundary propagator in dimensional form is found to be

$$G'(x^*, t^*) = \frac{x^*}{\sqrt{4\pi\kappa t^{*3}}} \exp\left(-\frac{(x^* - vt^*)^2}{4\kappa t^*} \right). \tag{16}$$

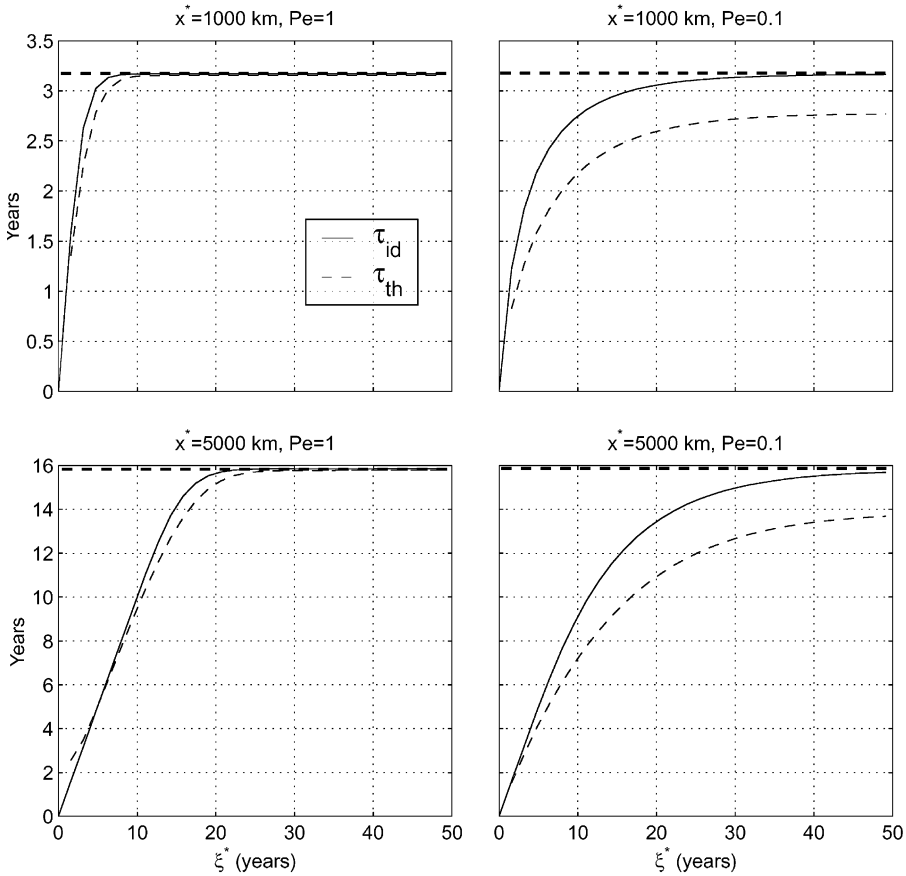

Fig. 2. Transient evolution of τ_{id} and τ_{th} in a 1-d advection–diffusion model showing the approach to a steady state. The upper panels show the response at $x^* = 1000$ km for two different values of Pe. The lower panels show the same, but at $x^* = 5000$ km. The thick horizontal dashed line is the mean age computed from the transit-time PDF.

In the rest of this section, dimensional variables will be superscripted with an $*$. The *mean age* (τ_{m}) is defined as the first moment of the transit-time PDF:

$$\tau_{\mathrm{m}}(x^*) = \int_0^\infty \xi^* \mathscr{G}'(x^*, \xi^*)\,\mathrm{d}\xi^*. \tag{17}$$

In this example, $\tau_{\mathrm{m}}(x^*) = x^*/v$. Fig. 2 shows the time evolution of τ_{th} and τ_{id} at $x = 10$ ($x^* = 1000$ km for $L = 100$ km) and $x = 50$ ($x^* = 5000$ km) for Pe $= 1$ and 0.1, respectively. Note how the ideal age approaches the mean age, τ_{m} (Eq. (17)). The generality of this result has been noted by Boering et al. (1996) and is easily demonstrated as follows. In steady state, the ideal age obeys

$$\mathscr{L}(\tau_{\mathrm{id}}(\mathbf{x})) = 1 \tag{18}$$

with $\tau_{\mathrm{id}}(\mathbf{x}) = 0$ on $\partial\mathscr{D}$. $\mathscr{L}$ is the stationary transport operator. The age spectrum satisfies

$$\frac{\partial \mathscr{G}'}{\partial t} + \mathscr{L}(\mathscr{G}') = 0$$

with $\mathscr{G}'(\mathbf{x}, t) = \delta(t)$ on $\partial\mathscr{D}$. Multiplying the above equation with t, integrating with respect to t, and making use of the normalization condition (Eq. (12)), we get

$$\mathscr{L}\int_0^\infty t\mathscr{G}'\,\mathrm{d}t = \mathscr{L}(\tau_{\mathrm{m}}) = 1$$

with $\tau_{\mathrm{m}}(\mathbf{x}) = 0$ on $\partial\mathscr{D}$. Since τ_{m} satisfies the same linear differential equation and boundary conditions as $\tau_{\mathrm{id}}(t \to \infty)$ (Eq. (18)), by uniqueness $\tau_{\mathrm{m}} = \tau_{\mathrm{id}}(t \to \infty)$. For completeness, we note that Hall and Plumb (1994) have shown that for a boundary condition of linearly increasing tracer concentration ($C_{\mathrm{o}}(t) = \gamma t$ in Eq. (14)), the tracer concentration in the long-time limit is related to the mean age by

$$C(\mathbf{x}, t) = \gamma(t - \tau_{\mathrm{m}}(\mathbf{x})).$$

The other feature to note is how different the two age tracers are for the more diffusive case (Pe = 0.1), consistent with what was predicted above, i.e., $\tau_{\mathrm{th}} < \tau_{\mathrm{id}}$. Furthermore, in the presence of greater diffusion the age tracers take longer to reach a steady state, an important consideration

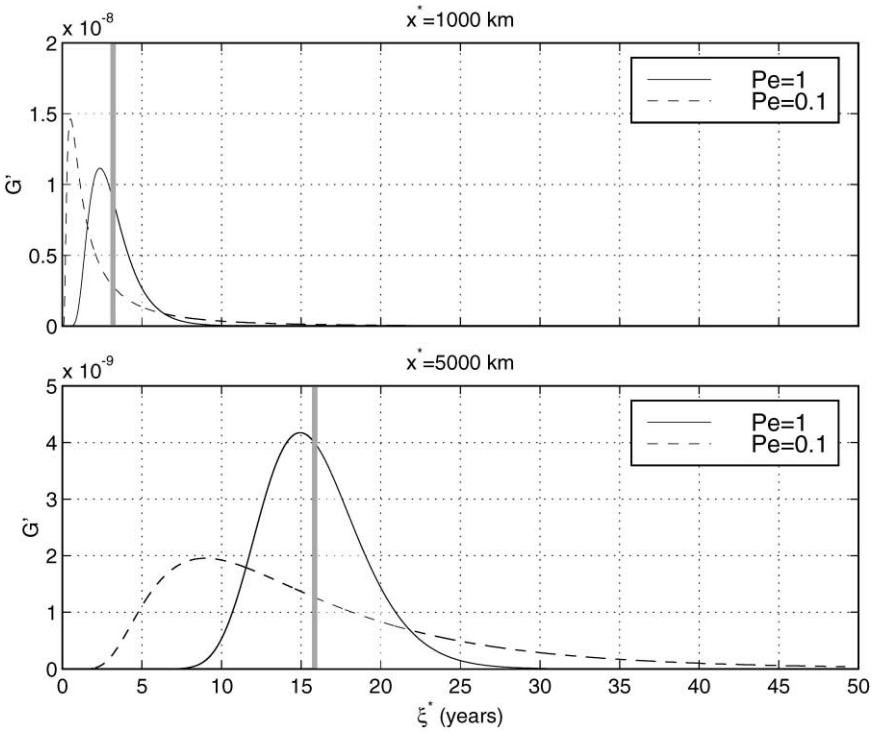

Fig. 3. Transit-time PDF plotted as a function of elapsed time ξ^* at $x^* = 1000$ km (upper) and $x^* = 5000$ km (lower) for Pe = 1 and 0.1. Vertical lines represent the mean age (τ_{m}) which in this case is independent of Pe.

when age tracers are simulated in numerical models. The transit-time PDF at various locations is plotted in Fig. 3 for different Peclet numbers. The important feature here is that consistent with its interpretation, in the more diffusive case the transit-time PDF $\mathscr{G}'(x^*, \xi^*)$ has a longer "tail". With increasing diffusion, there are more pathways by which a particle can reach any given point from the boundary. Peculiar to this 1-d case the mean age (τ_m) is independent of the Peclet number (vertical lines in Fig. 3), but this is in general not true and the long tails can significantly influence the mean age.

5. Simulations in an ocean GCM

To study the ideas discussed above in a more realistic setting, we have simulated ^{3}H, ^{3}He, τ_{id}, and $\mathscr{G}'$ in the Lamont ocean–atmosphere model (LOAM), an ocean GCM. The model domain spans the Atlantic Ocean between 30°S and 73°N at 2° resolution in the horizontal. The ocean component has 30 fixed vertical levels, with resolution ranging from 15 to 250 m. Unresolved processes are parameterized by a bulk wind-driven mixed layer model, convective adjustment, and isopycnal thickness diffusion (Gent and McWilliams, 1990). The model is coupled to an atmospheric boundary layer model (Seager et al., 1995) which supplies surface fluxes of heat. Freshwater fluxes are provided by restoring the sea surface salinity to the Levitus climatology (Levitus et al., 1994). The boundary layer atmospheric temperature and humidity are specified over land (from the ECMWF data set) but vary over the ocean according to an advective–diffusive balance subject to air–sea fluxes. All other boundary conditions such as the short-wave radiation (ISCCP), cloud cover (ISCCP), wind speed, vector, and stress (ECMWF) are specified at each grid point with monthly resolution. At the northern and southern boundaries, the ocean temperature and salinity are restored to the Levitus climatology.

5.1. Tracer equations and boundary conditions

The OGCM integrates the advection–diffusion equation with a general source term, $Q(C, \mathbf{x}, t)$,

$$\frac{\partial C}{\partial t} + \mathscr{L}(C) = Q(C, \mathbf{x}, t). \tag{19}$$

Source functions were specified as follows:

^{3}H: $Q = -[^3\mathrm{H}]\lambda$

^{3}He: $Q = [^3\mathrm{H}]\lambda$

τ_{id}: $Q = 1$

The tracers also satisfy the following initial and boundary conditions:

Initial conditions: $[^3\mathrm{H}] = 0$, $[^3\mathrm{He}] = 0$, and $\tau_{id} = 0$ at $t = 0$.

Boundary conditions: $[^3\mathrm{H}] \to 1$, $[^3\mathrm{He}] \to 0$, and $\tau_{id} \to 0$ at the surface ($z = 0$).

All passive tracers satisfy no-flux conditions at the northern and southern boundaries of the domain.

The transit-time PDF also satisfies Eq. (19) with $Q = 0$. From Eq. (13) we see that $\mathscr{G}'(\mathbf{x}, t; \partial\mathscr{D}, t')$ satisfies an impulse boundary condition. Here $\partial\mathscr{D}$ is the surface of the ocean, and thus $\mathscr{G}'(\mathbf{x}, t; \partial\mathscr{D}, t') = \delta(t - t')$ when $\mathbf{x}$ is on the surface. In the near-surface ocean and in regions of deep

convection there is strong seasonality in the transport operator and $\mathscr{G}'(\mathbf{x}, t; \partial\mathscr{D}, t')$ will depend on t' in some complicated manner. For example, an impulse applied in January could well have a different response than one applied in August. While it would be interesting to study the effect of the non-stationarity of the transport on the transit-time PDF, to minimize computational expense we will neglect the non-stationarity of the transport, implying that $\mathscr{G}'(\mathbf{x}, t; \partial\mathscr{D}, t') = \mathscr{G}'(\mathbf{x}, \xi; \partial\mathscr{D})$, where $\xi \equiv t - t'$ is the elapsed time. $\mathscr{G}'(\mathbf{x}, \xi; \partial\mathscr{D})$ is then the PDF of elapsed time since water at $\mathbf{x}$ last made contact with the surface of the ocean. Furthermore, to "smooth" out the seasonality at the surface, the impulse BC is approximated as

$$\mathscr{G}'(\mathbf{x}, \xi; \partial\mathscr{D}) = \begin{cases} 1/N_s, & 0 \leqslant \xi \leqslant 1 \text{ yr}, \\ 0, & \xi > 1 \text{ yr}, \end{cases}$$

where N_s is the number of seconds in 1 yr. In practice, the surface concentration for $0 \leqslant \xi \leqslant 1$ yr is set to 1 (rather than $1/N_s$), and the response is divided by N_s to recover the transit-time PDF, $\mathscr{G}'(\mathbf{x}, \xi; \partial\mathscr{D})$.

5.2. Results

Dynamical fields were first allowed to spin-up during a 200-yr integration of the OGCM, after which tracers were introduced and the model integrated for a further 200 yr. Results from the latter 200-yr integration of the OGCM are used in this study. As we discuss below, even in our limited domain this is clearly too short a time for steady-state to be reached (e.g. England, 1995), but our goal here is to gain insight into the behavior of various age tracers and not to achieve a realistic simulation.

5.2.1. Transit-time PDF

To gain some insight into the transit-time PDF, we begin by displaying maps of its *column integral* at various times (Fig. 4). In particular, we wish to illustrate the influence of an impulse *boundary condition* on passive tracers such as the boundary propagator or transit-time PDF. The top four panels in Fig. 4 show the column inventory at 6-month intervals starting at time $t = 0^+$ (January). Recall that the "impulse" is applied for an entire year, during which the surface acts as a source of tracer. Six months into the model integration ($t = 0.5$) deep convection has increased the column inventory in the Labrador and Irminger seas. There is also a hint of this in the subtropical subduction region. Keep in mind that the maps have been normalized to their respective maximum values and hence should not be compared with each other. At the end of the first year ($t = 1$) the impulse is "turned off" and the surface now acts as a sink of tracer. Subsequently, deep convection has the effect of "sucking out" tracer from the ocean as is clearly seen at $t = 1.5$. Any tracer which has entered the ocean during the first year will be advected and diffused around. The other panels in Fig. 4 show how the tracer plume spreads into the ocean, particularly along the western boundary. At the "trailing" (northern) edge of the plume, the tracer is being continuously diluted by mixing with recently ventilated water which due to the impulse boundary condition has a much lower tracer concentration. Indeed, because of diffusion, tracer is continuously removed from the ocean by ventilation.

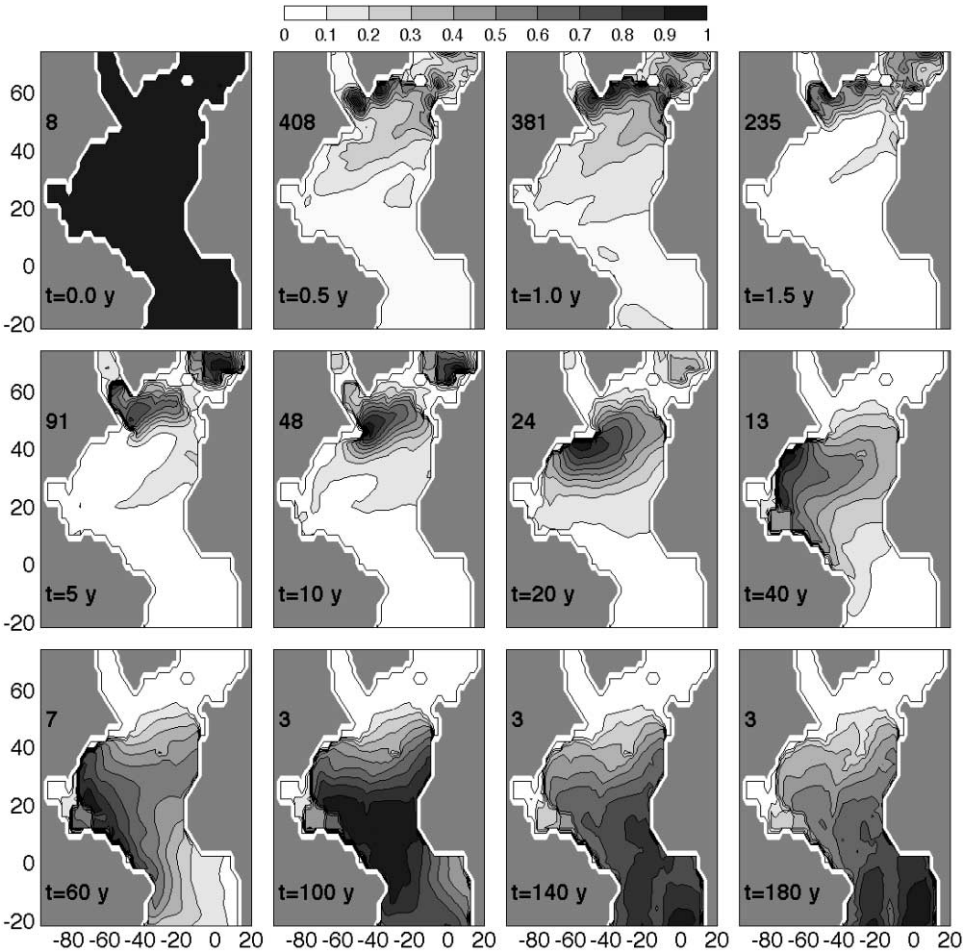

Fig. 4. Distribution of the column-integrated transit-time PDF at various times. The maps have been normalized to the maximum value of the column integral which is shown ($\times 10^{-7}$) in the upper left corner of each plot.

5.2.2. Comparison of transit-time PDF with tracer-derived ages

Next, we compare the spatial distribution of τ_{id}, τ_{th}, and τ_{m} at the end of the 200-yr model run. One potential problem which hinders the interpretation of ages derived from tracer observations as well as from simulations in numerical models is that the tracers are not in steady state, and we are only looking at the transient response. Indeed, the ideal age distribution obtained in the model is only meaningful in a steady state. On the other hand, it is the transient solution (to a δ BC at the surface) which is directly interpreted as the transit-time PDF. For the entire ocean, the approach to a steady state could take thousands of years (England, 1995). A useful measure of the degree to which the tracers are in steady state is the time integral of the transit-time PDF:

$$I(\mathbf{x}, t) = \int_0^t \mathrm{d}\xi \mathscr{G}'(\mathbf{x}, \xi; \partial\mathscr{D}).$$

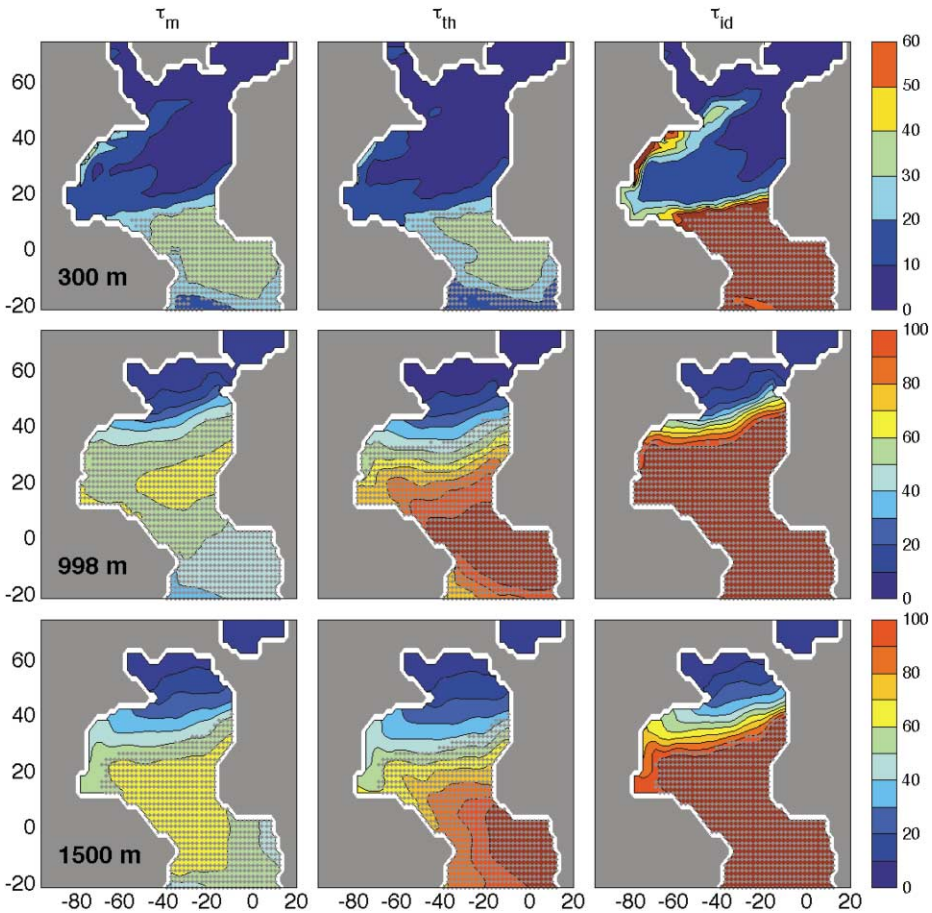

Fig. 5. Horizontal distribution of τ_m, τ_{th}, and τ_{id} in an OGCM integrated for 200 yr at 300 m (top), 1000 m (middle) and 1500 m (bottom). Grid points with $I < 0.8$ have been stippled.

Recall that $I(\mathbf{x}, t \to \infty) = 1$ (Eq. (12)), and thus for locations where $I(\mathbf{x}, t) \ll 1$ we do not expect the tracer-derived ages to be "reliable".

Fig. 5 shows the distribution of the mean age (τ_m), ^3H–^3He age (τ_{th}), and ideal age (τ_{id}) at 300, 1000, and 1500 m in the OGCM. Grid points where $I(\mathbf{x}, t)$ is less than some cutoff value, I_c, have been shaded. Somewhat arbitrarily we set $I_c = 0.8$. Only grid points where $I(\mathbf{x}, t) \geqslant I_c$ should be considered "reliable". Clearly, much of the ocean basin is not yet in steady state with respect to the transit-time PDF. The spatial distributions of all age tracers are fairly similar. In particular, the ideal age increases with depth as well as from north to south. The latter reflects the fact that the model ocean is ventilated from the north. The low ages in the subpolar and subtropical regions are due to ventilation by convection and subduction, respectively. At deeper levels, the pathways along which newly ventilated Labrador Sea Water spreads into the North Atlantic are clearly visible. The zone of high tracer age along the western boundary is due to upwelling in the model

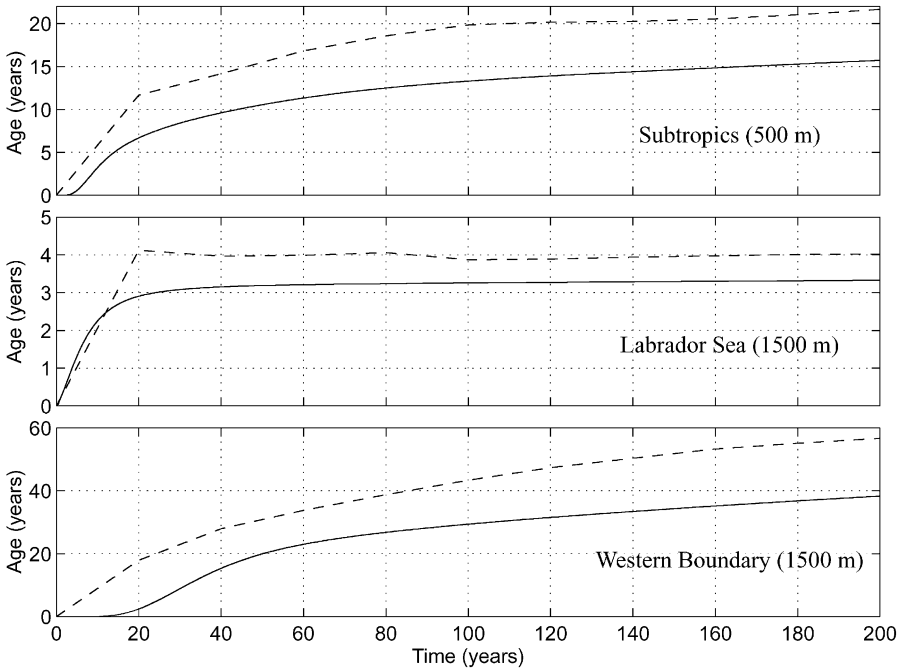

Fig. 6. Ideal age (dashed line) and cumulative first moment of transit-time PDF (solid line) as a function of elapsed time at three locations in the North Atlantic: Labrador Sea (57°N, 52°W, 1500 m), subtropical subduction region (37°N, 26°W, 500 m), and western boundary (37°N, 64°W, 1500 m). The locations are indicated on the inset map in Fig. 7.

which brings up tracer-free water. This has the greatest impact on τ_{id} because the upwelling brings up relatively old water. In contrast, the upwelling water has a much lower transit-time PDF "concentration" thus lowering the mean age. The simulations also confirm the predicted relationship, $\tau_{\mathrm{th}} < \tau_{\mathrm{id}}$. Interestingly, the mean age is consistently younger than the ideal age. In steady state the two will be equal, but apparently the transit-time PDF has a rather long "tail" (due to diffusion). Thus, even though the "diffusive" long transit-time pathways make up only a small fraction of a water parcel, they could disproportionately influence its first moment (τ_{m}). The slow "convergence" (long tail) of the transit-time PDF is of practical importance, since if we are only interested in the mean age, it might be more efficient to simulate the ideal age tracer to a steady state rather than computing τ_{m} as the first moment of the transit-time PDF (Eq. (17)). To further emphasize this slow convergence, Fig. 6 compares the "cumulative" first moment of the transit-time PDF ($\int_0^t \xi \mathscr{G}'(\mathbf{x}, \xi; \partial\mathscr{D})\,\mathrm{d}\xi$) with the ideal age at three locations in the North Atlantic. Recall that in the long-time limit, the cumulative first moment converges to the mean age (by definition).

Consider now the transit-time PDF at various locations. The upper panel in Fig. 7 shows the transit-time PDF as a function of time at the same three locations (indicated on the inset map) in the North Atlantic. The PDF's have been normalized to their maximum value to fit them on the same vertical axis. The lower panel shows their time integral, $I(\mathbf{x}, t)$, at those same locations. The transit-time PDF in the Labrador Sea (at 1500 m) shows considerable seasonal variability because

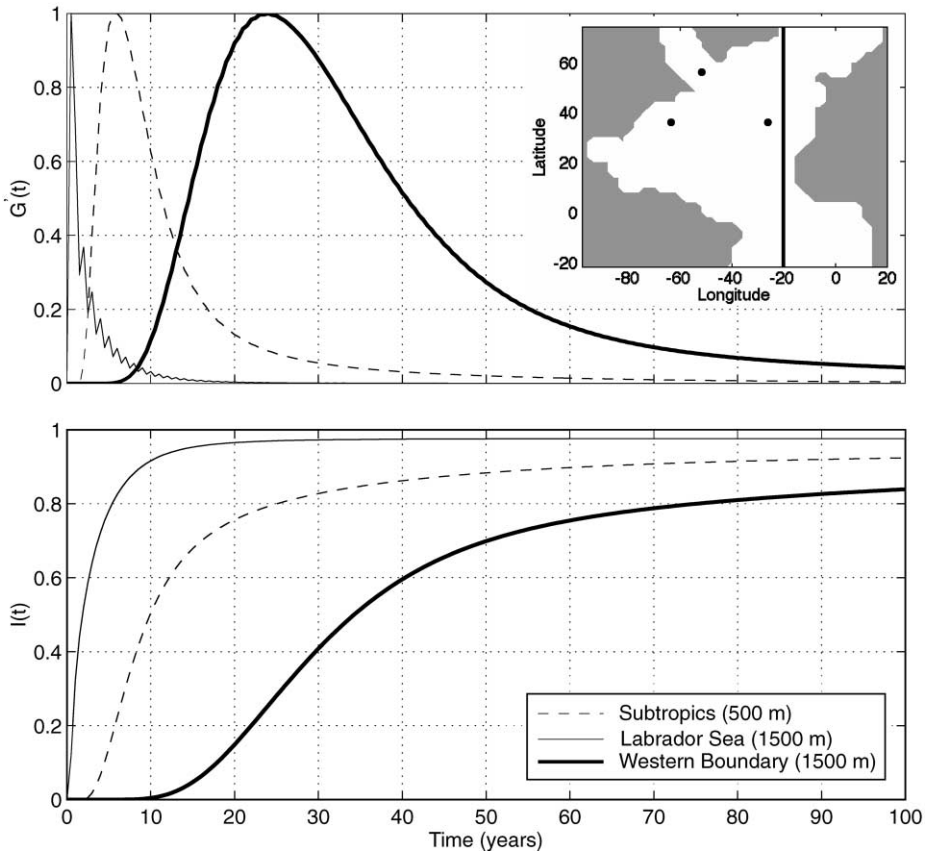

Fig. 7. Transit-time PDFs (upper panel) as a function of elapsed time at three locations in the North Atlantic: Labrador Sea (57°N, 52°W, 1500 m), subtropical subduction region (37°N, 26°W, 500 m), and western boundary (37°N, 64°W, 1500 m). PDFs have been normalized by their maximum values. The inset map on the upper panel shows the position of the three locations as well as that of the section shown in Fig. 8. The lower panel shows the time integral, $I(\mathbf{x}, t)$, at the same locations.

of deep convection and the age spectrum is sharply peaked towards young ages. The strong non-stationarity in the transport is some cause for concern. The subtropical subduction region (500 m) also shows a relatively sharp peak but a longer "diffusive" tail. At the western boundary location, the PDF is even more spread out due to mixing with tracer-free water. A comparison of the different age measures at the three locations is presented in Table 2. Some caution is required in interpreting the ages in the Labrador Sea because of the strong seasonality. At the other locations this is not a problem. Note that near the western boundary τ_m is considerably younger than τ_{id}, but because of the extended tail, it is expected that contributions from very long transit times will significantly increase the mean age at that location.

It is useful to compare the simulated ^3H–^3He ages with observations. The upper panel in Fig. 8 shows the meridional distribution of τ_{th} in the eastern North Atlantic nominally along 20°W as

Table 2
Comparison of various age measures at three locations in a numerical model of the Atlantic Ocean at the end of a 200-yr integration

Location	$I(\mathbf{x}, 200)$	τ_m	τ_{id}	τ_{th}
Labrador Sea (1500 m)	0.98	3.3	4	3.9
Subtropical subduction region (500 m)	0.94	15.8	21.7	12.8
Western boundary (1500 m)	0.9	38.4	56.7	35.8

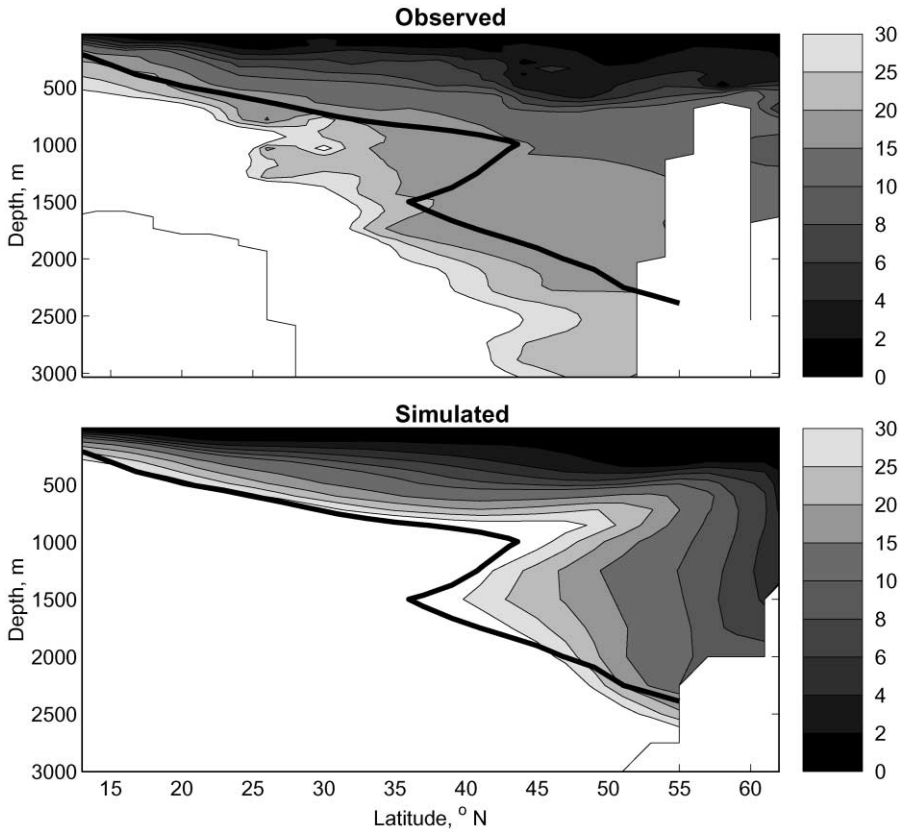

Fig. 8. Meridional distribution of τ_{th} in the eastern North Atlantic from observations (upper panel) and simulated in the OGCM (lower panel). Thick black line is the $I = 0.8$ contour.

reported by Doney et al. (1997). The lower panel shows the τ_{th} simulated in the OGCM at the same longitude. The thick black line is the $I = 0.8$ contour; I *decreases* below this line. Differences between observed and simulated ages can be ascribed to the idealized nature of the surface boundary condition for ^{3}He, as well as the absence of a Mediterranean basin in the model. The overall pattern of penetration of newly ventilated water is, however, reasonably well captured by the model.

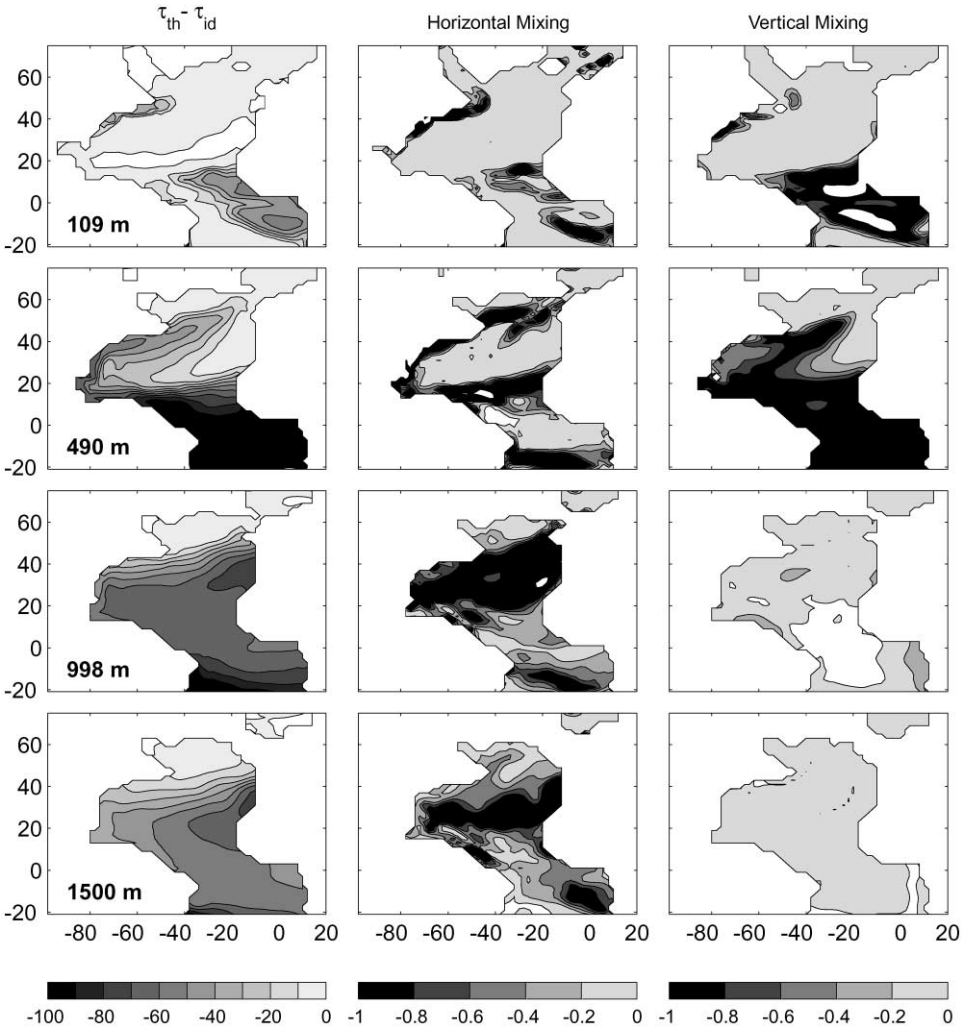

Fig. 9. Spatial distribution of $\tau_{th} - \tau_{id}$ (left column), horizontal mixing term (center), and vertical mixing term (right) at various depths.

5.2.3. *Effect of mixing on ages*

Recall that the advection–diffusion equation for ^3H–^3He age (Eq. (4)) contains two additional terms in comparison with the ideal age equation (Eq. (2)). These terms describe isopycnal and diapycnal non-linear mixing effects which give rise to differences between τ_{th} and τ_{id}. To quantify the effect of non-linear mixing, we have diagnosed the magnitude of these terms in the OGCM. For simplicity, we have ignored the inclination of isopycnals from the horizontal. In the very northern part of the domain this is clearly a bad approximation, but our goal here is to compare ages away from the convective regions where isopycnals are nearly horizontal. We have also assumed nominal values of 10^3 and $10^{-5}\,m^2\,s^{-1}$ for the horizontal and vertical diffusivities, respectively. Fig. 9 (left)

shows the spatial distribution of the difference field $\tau_{th} - \tau_{id}$ at various depths. The middle and right columns in Fig. 9 show the corresponding distribution of the diagnosed horizontal ($\kappa_h \mathbf{\nabla}_h \ln([^3H]\zeta) \cdot \mathbf{\nabla}_h \tau_{th}$) and vertical ($\kappa_v(\partial \ln([^3H]\zeta)/\partial z)\partial \tau_{th}/\partial z$) mixing terms. The first point to note is that the mixing terms are negative and of $O(1)$. The fact that the size of the mixing terms is comparable to that of the main "source" term ("1") in the age equations implies that the effect of mixing on transient-tracer ages is potentially very important. Interestingly, the age difference ($\tau_{th} - \tau_{id}$) is relatively small in the subtropical subduction region, where both vertical and horizontal mixing terms are small. This result is consistent with field data (Jenkins, 1987) from the North Atlantic. Next compare the relative contributions of the vertical and horizontal mixing terms to the age difference. Evidently in the upper part of the water column, vertical mixing dominates the age difference. As we go deeper, the horizontal term becomes more important and correlates with maximum age differences. This trend reflects the fact that in the upper ocean vertical gradients are larger, and tracers penetrate by vertical mixing. On the other hand, in the deep ocean tracer gradients are larger along the isopycnals, reflecting ventilation of the deep ocean along the isopycnals.

Acknowledgements

SK and PS were supported by NOAA Grants NA46GP0112 and NA86GP0375. MV was funded by NOAA Grant NA86GP0301 and ONR Grant N00014-98-1-0302. Tim Hall generously shared his insight into the mathematics of tracers. We thank Marc Spiegelman for useful discussions, Naomi Naik for helping with the numerical calculations, Scott Doney for making available the tritium and helium data shown in Fig. 8, and two anonymous referees for providing useful suggestions to improve the text. Lamont–Doherty Earth Observatory contribution 6112.

References

Abramowitz, M., Stegun, I.A. (Eds.), 1965. Handbook of Mathematical Functions. Dover, New York.

Beining, P., Roether, W., 1996. Temporal evolution of CFC 11 and CFC 12 in the ocean interior. Journal of Geophysical Research 101, 16,455–16,464.

Boering, K.A., Wofsy, S.C., Daube, B.C., Schneider, H.R., Loewenstein, M., Podolske, J.R., Conway, T.J., 1996. Stratospheric mean ages and transport rates from observations of carbon dioxide and nitrous oxide. Science 274, 1340–1343.

Bolin, B., Rodhe, H., 1973. A note on the concepts of age distribution and transit time in natural reservoirs. Tellus 25, 58–62.

Doney, S.C., Jenkins, W.J., Bullister, J.L., 1997. A comparison of tracer dating techniques on a meridional section across the eastern North Atlantic. Deep-Sea Research I 44, 603–626.

England, M.H., 1995. The age of water and ventilation timescales in a global ocean model. Journal of Physical Oceanography 25, 2756–2777.

Gent, P.R., McWilliams, J.C., 1990. Isopycnal mixing in ocean circulation models. Journal of Physical Oceanography 20, 150–155.

Hall, T.M., Plumb, R.A., 1994. Age as a diagnostic of stratospheric transport. Journal of Geophysical Research 99, 1059–1070.

Holzer, M., Hall, T.M., 2000. Transit-time and tracer-age distributions in geophysical flows. Journal of Atmospheric Science 57, 3539–3558.

IAEA, 1986. Mathematical models for interpretation of tracer data in groundwater hydrology. IAEA-TECDOC-381, International Atomic Energy Agency.

Jenkins, W.J., 1987. ^{3}H and ^{3}He in the beta triangle: observations of gyre ventilation and oxygen utilization rates. Journal of Physical Oceanography 17, 763–783.

Jenkins, W.J., 1998. Studying subtropical thermocline ventilation and circulation using tritium and ^{3}He. Journal of Geophysical Research 103, 15,817–15,831.

Jenkins, W.J., Clarke, W.B., 1976. The distribution of ^{3}He in the western Atlantic Ocean. Deep-Sea Research 23, 481–494.

Kida, H., 1983. General circulation of air parcels and transport characteristics derived from a hemispheric gcm, Part 2. Very long-term motions of air parcels in the troposphere and stratosphere. Journal of the Meteorological Society of Japan 61, 510–522.

Levitus, S., Burgett, R., Boyer, T.P., 1994. World Ocean Atlas 1994, vol. 3: Salinity. NOAA Atlas NESDIS 3, U.S. Government Printing Office, Washington, DC, 99pp.

Morse, P.M., Feshbach, H., 1953. Methods of Theoretical Physics. McGraw-Hill, New York.

Nir, A., Lewis, S., 1975. On tracer theory in geophysical systems in the steady and non-steady state. Part I. Tellus 27, 372–383.

Seager, R., Blumenthal, M.B., Kushnir, Y., 1995. An advective atmospheric mixed-layer model for ocean modeling purposes — global simulation of surface heat fluxes. Journal of Climatology 8, 1951–1964.

Thiele, G., Sarmiento, J.L., 1990. Tracer dating and ocean ventilation. Journal of Geophysical Research 95, 9377–9391.

Unterweger, M.P., Coursey, B.M., Schima, F.J., Mann, W.B., 1980. Preparation and calibration of the 1978 National Bureau of Standards tritiated-water standards. International Journal of Applied Radiation and Isotopes 31, 611–614.